

Unveiling the nature of the “Green Pea” galaxies

R. O. Amorín, J. M. Vílchez and E. Pérez-Montero

Abstract We review recent results on the oxygen and nitrogen chemical abundances in extremely compact, low-mass starburst galaxies at redshifts between 0.1-0.3 recently named to as “Green Pea” galaxies. These galaxies are genuine metal-poor galaxies (\sim one fifth solar in median) with N/O ratios unusually high for galaxies of the same metallicity. In combination with their known general properties, i.e., size, stellar mass and star-formation rate, these findings suggest that these objects could be experiencing a short and extreme phase in their evolution. The possible action of both recent and massive inflow of gas, as well as stellar feedback mechanisms are discussed here as main drivers of the starburst activity and their oxygen and nitrogen abundances.

1 Introduction

There is strong evidence that compact low-mass starburst galaxies with properties similar to those of Blue Compact Galaxies (BCGs) have provided $\sim 40\%$ of the star formation rate (SFR) density at redshift $z = 1$ [1]. The idea of a strong evolution of low-mass galaxies at a relatively late cosmic epoch (i.e., by the time when the Universe has been half of the present age) is consistent with “downsizing” scenarios of galaxy formation, predicting a strong evolution with specific SFR progressing from high- to low-mass systems with time [2]. The rapid decline of these proto-BCGs from $z = 1$ to $z = 0$ and subsequent evolution are barely understood.

One of the largest and most homogeneous samples of low-mass starbursts at redshift $z < 1$, is the commonly referred to as “Green Pea” (GP) galaxies, recently discovered by their unusual color and compact size (unresolved on SDSS images) by the “Galaxy Zoo” project [3], and further studied in some detail by [4], [5], and

R. O. Amorín (e-mail: amorin@iaa.es); J. M. Vílchez (e-mail: jvm@iaa.es); E. Pérez-Montero (e-mail: epm@iaa.es)

Instituto de Astrofísica de Andalucía, Glorieta de la Astronomía S/N, Granada, Spain

[6]. The GPs are mainly located in lower-density environments and are spectroscopically characterized by very faint continuum emission and strong optical emission lines, such as the [O III] $\lambda 5007$ emission line, with an unusually large equivalent width of up to ~ 2000 Å. According to the above studies, at least 80 of these newly discovered objects are very compact (half-light radius $\sim 1-2$ kpc) low-mass ($M_* \sim 10^8 - 10^{10} M_\odot$) starbursting systems (SFRs up to $60 M_\odot \text{ yr}^{-1}$, as derived from their $H\alpha$ and UV luminosities). The above properties led to the conclusion that the GPs are identifiable with the high-luminosity end of nearby BCGs, probably representing earlier and extreme stages of BCG evolution. Moreover, their extremely high specific SFRs ($10^{-9} - 10^{-7} \text{ yr}^{-1}$) are among the highest known in the nearby Universe, and comparable to those of high redshift galaxies. The similarities in these properties, and also – as we will see below – those found in their chemical abundances and extinction suggest physical conditions that largely resemble those in galaxies in the early Universe. Therefore, the GPs may be used as nearby proxies for studying in much greater detail the stellar mass growth of galaxies and the physical processes involved in the triggering of violent star formation and the chemical evolution of higher-redshift galaxies.

2 Oxygen and nitrogen chemical abundances and scaling relations

In [5] we used SDSS spectra to carry out a detailed study of the chemical abundances of the sample of GPs in the redshift range $0.11 \leq z \leq 0.36$ that were spectroscopically classified as star-forming systems by [4]. We measured emission-line integrated fluxes for all galaxies after a linear subtraction of the continuum and then we computed their oxygen total abundances and nitrogen-to-oxygen ratios, N/O, using empirical methods ($N2 \equiv \log([N \text{ II}] \lambda 6584/H\alpha)$ and $N2S2 \equiv [N \text{ II}]/[S \text{ II}]$ [7]). Additionally, for a subset of galaxies with reliable measurements of the [O III] $\lambda 4363$ emission line (70% of the sample) physical properties and oxygen and nitrogen ionic abundances were calculated using the more reliable direct method.

In contrast to [4], our results showed that the GPs are a population of genuinely metal-poor galaxies, with oxygen abundances $7.7 \leq 12 + \log(O/H) \leq 8.4$ (mean value of 8.05 ± 0.14 , or $\sim 20\%$ the solar value). This value is ~ 0.65 dex lower than that previously obtained by [4] using an empirical calibration based on the $[N \text{ II}]/[O \text{ II}]$ ratio. This large difference was attributed by [5] to the dependence of $[N \text{ II}]/[O \text{ II}]$ on the variation of the N/O ratio at a given O/H, since large values of N/O can enhance $[N \text{ II}]/[O \text{ II}]$ even in the low-metallicity regime [7]. As we shall show below, the N/O values displayed by the GPs are higher than expected for their metallicity. It is worth noting that our direct and empirical estimates of the oxygen and nitrogen abundances agree well within the typical uncertainties (~ 0.1 dex). The GPs were also found to show relatively low extinction, with $C(H\beta)$ and $H\alpha/H\beta$ mean values 0.23 and 3.3, respectively. This confirms that these objects should be relatively dust free.

Fig. 1 N/O vs. O/H abundance ratio. The 2D histogram of SDSS SFGs is shown in logarithmic scale while the GPs are indicated by circles.

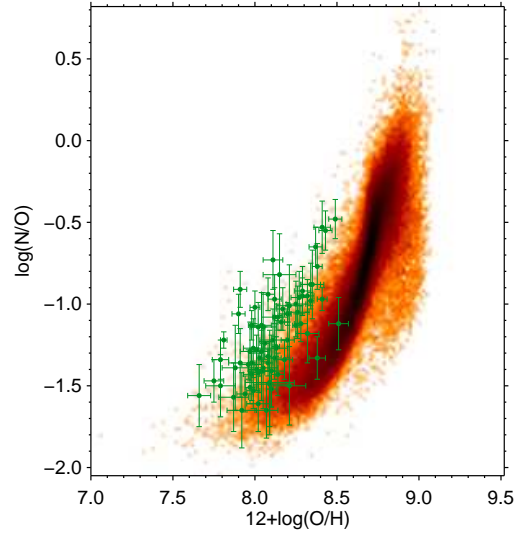
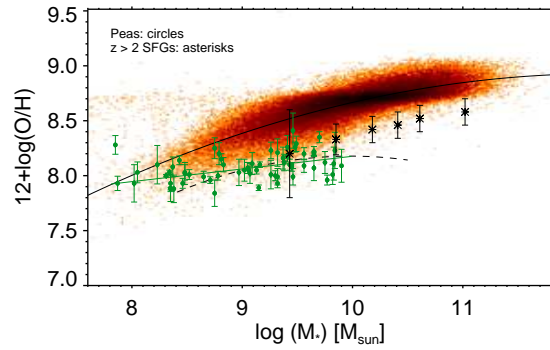


Fig. 2 O/H vs. stellar mass. The 2D histogram of SDSS SFGs is shown in logarithmic scale and their best likelihood fit is shown by a black solid line. The subset of 62 GPs (see text) are indicated by circles and their best linear fit is shown by a dashed line. For comparison we also show the quadratic fit presented in [5] for the full sample of 80 GPs. SFGs at $z \geq 2$ by [9] are also shown by asterisks for comparison.



The above results become even more interesting when compared with those of a statistically significant sample of star-forming galaxies (SFGs, taken from the MPA/JHU Data catalog of the SDSS DR 7), for which we have applied the same methods and calibrations. For both GPs and SDSS SFGs, we plot the relation between N/O and metallicity, the mass-metallicity relation (MZR) and the relation between N/O and the stellar mass in Fig. 1, Fig. 2 and Fig. 3, respectively. The two main results apparent from these figures will be the subject of our next discussion:

(1) in the low-to-intermediate metallicity range most GPs present systematically larger N/O ratios for a given metallicity compared to the SDSS SFGs (Fig. 1).

(2) while most GPs show N/O ratios roughly consistent with the relation with stellar mass of local SFGs (Fig. 3), we find that the MZR of the GPs is systematically shifted to lower metallicities (Fig. 2).

Fig. 3 N/O vs. stellar mass. Symbols are the same as in Fig. 1.

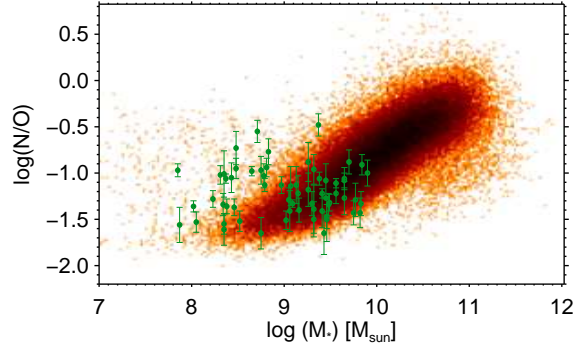
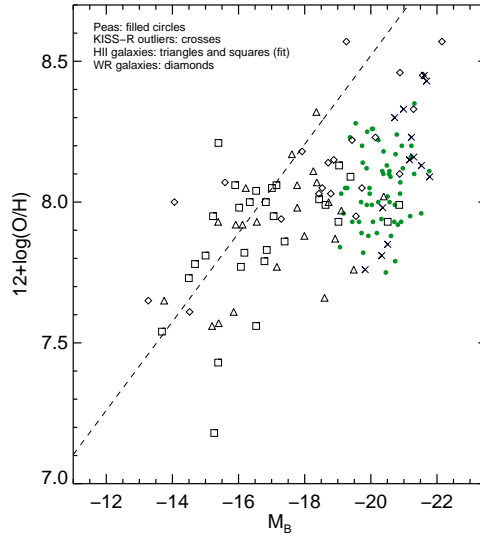


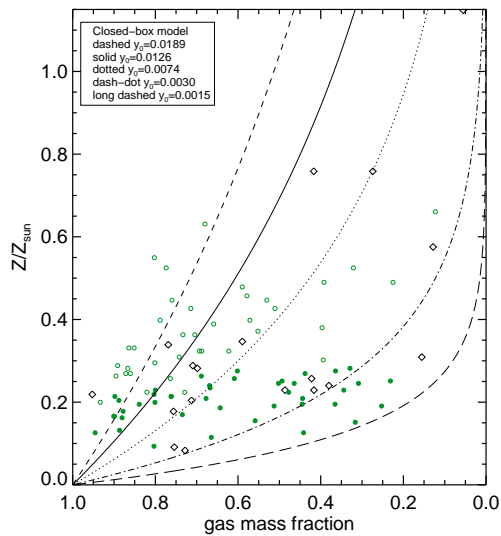
Fig. 4 O/H vs. B-band (rest-frame) absolute magnitude. The meaning of symbols is indicated. Distances used in computing (extinction-corrected) absolute magnitudes were, in all cases, calculated using spectroscopic redshifts and the same cosmological parameters. The dashed line indicates the fit to the HII galaxies in the MLR given by [12].



Figures 2 and 3 are similar to those presented in [5]. However, instead of using M_* derived by [4] (i.e., fitting the spectral energy distribution from SDSS photometry after subtracting the contribution of emission lines), here we have used a more reliable estimation of M_* recently obtained by [6]. For 62 out of 80 GPs, they derived M_* from fitting their SDSS spectra after subtracting the contribution of both the nebular continuum emission and the line emission. On average, these new stellar mass estimates are by ~ 0.35 dex lower than that of [4]. However, a comparison of our previous fit in [5] with our fit using the new M_* values in Fig. 2 (dashed and solid line, respectively) shows that the original overestimation of M_* is not large enough to explain the offset between GPs and SDSS SFGs. Only in the lower mass (luminosity) regime, where galaxies have SDSS spectra with much poorer S/N and therefore are subject of larger uncertainties in the spectral fitting, the GPs seem to match the trend of the local SDSS SFGs.

According to their main properties (i.e., stellar mass, size, SFR, metallicity) the GPs appear to bear close resemblance to other, smaller samples of strongly star

Fig. 5 Gas mass fraction vs. metallicity. Different lines correspond to closed-box models at different yields, as indicated in the legend. Open and filled circles are GPs which are above and below the fit to their MZR in [5], respectively. Diamonds are values for the same WR galaxies as in Fig. 4.



forming galaxies at similar redshifts selected using different criteria. That is the case for some Lyman Break Analogs (LBAs) included in the analysis done by [5]. They are a subset of 30 local UV-luminous galaxies studied in detail by [8] (and references therein) which show strong similarities with the more distant Lyman Break Galaxies (LBGs), like those at $z > 2.2$ studied by [9] that are shown for comparison in Fig. 2. The low-metallicity “Ultra Strong Emission Line” galaxies found at redshift $z < 1$ by [10] or the luminous starburst galaxies at redshifts in the range 0.29-0.42 from the KISS survey discovered by [11], also show strong similarities with the GPs. Interestingly, the latter have been presented as extreme outliers in the mass-luminosity relation (MLR) as compared with the local Blue Compact/ HII galaxies in the KISS survey. In Fig. 4 we show their position and that of the GPs in the MLR. For comparison, we also added a sample of HII galaxies from [12] and a sample of highly interacting, local Wolf-Rayet (WR) galaxies by [13]. In Fig. 4, the GPs and the KISS outliers do not follow the linear relation established by the HII galaxies at lower luminosities, showing a clear offset of $\sim 2-3$ magnitudes. This difference in the luminosity-metallicity relation between strongly star-forming galaxies (including the sample of GPs) and local emission-line galaxies has been also shown by [6], who pointed out that the observed trend for GP-like objects is more similar to the one described by distant LBGs.

2.1 Comparison with the closed-box model

As a preliminary approach in studying our results in terms of chemical evolutionary models, in Fig. 5 we compare the observed oxygen abundance of the GPs as a

function of the gas mass fraction with the predictions of the simplest, closed-box model, that assumes the galaxies as closed systems, with no inflows or outflows, in addition to instantaneous recycling and a constant SFR. In this model the metallicity is written as $Z = y_0 \ln(1/\mu)$, where y_0 is the true yield by mass, and μ is the gas mass fraction. Since no HI observations are available for the GPs, the latter has to be calculated by assuming a star formation law. For doing so, we combined the correlation between surface gas density and SFR per unit area with the conversion from H α luminosity to SFR from the relations given by [14]. Since the GPs are unresolved in SDSS, in this approach we considered the area where neutral gas (involved in star formation) is located as the one defined by the size of the SDSS fiber (i.e., 3''). In Fig. 5 the lines indicate predictions of the model using different yields, where the black line represents a model with $y = 1Z_{\odot}$, while the red one is the theoretical oxygen yield expected for stars with rotation of [15], $y \sim 0.6Z_{\odot}$. Although part of the large dispersion in the GP values may be due to the large uncertainties introduced by the assumptions made on the gas mass fraction estimates, it seems clear that the closed-box model does not reproduce the overall trend of the GPs. This is especially remarkable in those GPs – indicated by filled circles – that show metallicities lower than the average given by the linear fit in Fig. 2. Fig. 4 suggests that more sophisticated models, including outflows of enriched gas and inflows of pristine gas, should be needed to better address the chemical evolution of the GPs.

3 Discussion

Feedback processes associated with the vigorous star formation taking place in the GPs can be invoked to explain the above results. Large amounts of supernovae (SNe) are expected to be produced by the starbursts on very short time scales. The enriched material produced by these SNe might escape from the galaxy, overcoming a relatively weak potential, diluting metal abundances and explaining the offset in the MZR. Simulations (e.g., [16]) and observations at low (e.g., [8]) and high redshift (e.g., [9]), have invoked SNe feedback to explain the shape of the MZR in low-mass star-forming galaxies. In contrast, analytical models by [17] show that any subsequent star formation event will remove a MZR offset, unless galaxies have an inefficient star formation.

A different view of the feedback processes comes from some analytical models and simulations (e.g., [18], [19]). They show that under some hydrodynamical conditions which are expected to be present in extremely compact, high specific SFR objects such as the GPs, the material ejected and accelerated by the SNe can cool down efficiently and be reinserted into the star-forming regions. This way, the enriched material never escapes from the galaxy and is reprocessed by successive generations of stars until most of the gas is transformed into new stars. This is the so-called ‘‘positive feedback’’, a process that would act in extremely short time scales and thus requires a high star formation efficiency. Positive feedback would explain the offset of the GPs in the MZR. However, some chemical evolution models (e.g.,

[20]) have shown that higher star formation efficiencies produce lower values in N/O at a given metallicity in the range $12 + \log(\text{O}/\text{H}) < 8.4$, which is the opposite to the observed trend on the N/O – O/H diagram (Fig. 1).

Given the similarities found between the GPs and starbursts at higher redshift, i.e., LBGs, an inflow scenario is especially interesting since it has recently been suggested that at redshift $z \sim 2 - 3$ (e.g., asterisks in Fig. 2) accretion of cold gas may be the main driver of star formation and stellar mass growth (e.g., [21], [22], [23]). Inflow of metal-poor gas, either from the outskirts of the galaxy or beyond, that can dilute metals in the galaxy centers [16], explaining the offset to lower abundances in the MZR and in the N/O – O/H diagram. In the models by [16], the dilution of metals due to an inflow can be restored by the effects of star formation depending on the dilution-to-dynamical timescale ratio. Since this ratio depends inversely with galaxy radius, galaxies with smaller radius, such as the GPs, may be expected to take longer time to enhance their oxygen abundances to the values expected from the MZR (predicted by the closed-box model).

Additional support to this scenario comes from the morphological analysis of few objects from spatially resolved HST images ([4,8]). These GPs show clumpy and disturbed morphologies probably associated with interactions/mergers. Recent accretion of cold gas can be due to interactions with small gas-rich galaxies or even large gas clouds. This eventually increases the gas surface density and consequently enhances the star formation. In models by [24] the rapid decrease of the oxygen abundance during an episode of massive and rapid accretion of metal-poor gas is followed by a slower evolution which leads to the closed-box relation, thus forming a loop in the N/O – O/H diagram. Under this model, the GPs would be at the first stages after infall triggers enhanced star formation, being very bright and moving slowly from the left to the right in Fig. 1, until the galaxies will finally arrive to the closed-box position. In order to reproduce the observed trends, further work might use these and other suitable models to quantify the relative importance of the accretion rates and/or the rate at which the galaxies expel enriched gas.

4 Conclusions

Green pea galaxies are a genuine population of metal-poor, luminous and very compact starburst galaxies. Results by [4], [5], and [6] permitted first clues to the evolutionary status of GPs. However, these galaxies and other similar samples in the local Universe should be analyzed in more detail to gain further insights into their nature, buildup process and evolutionary pathways. In particular, the direct assessment of the gas fraction, the refinement of the stellar mass estimations and their star formation history, as well as a proper comparison with detailed models of chemical evolution, are important issues to be addressed.

Recent deep and high signal-to-noise imaging and spectroscopic observations with OSIRIS at the 10-m. Gran Telescopio Canarias (GTC) (Amorín et al. 2011, in prep) will provide new insights on the evolutionary state of the GPs. In particular,

we will be able to see whether the GPs show an extended, old stellar population underlying the young burst, like those typically dominant in terms of stellar mass in most BCGs (e.g., [25], [26], [27]). The age, metallicity and mass of the old and young stellar populations will be analyzed in more detail by fitting population and evolutionary synthesis models to the observed spectra.

Acknowledgements We are very grateful to Polychronis Papaderos, Gerhard Hensler, and Simone Recchi for valuable comments on this manuscript. This work has been funded by grants AYA2007-67965-C03-02, and CSD2006-00070: First Science with the GTC (`\protect`<http://www.iac.es/consolider-ingenio-gtc/>) of the Consolider-Ingenio 2010 Program, by the Spanish MICINN.

References

1. Guzmán, R. et al., *ApJ* **489**, 559 (1997)
2. Cowie, L. L. et al., *AJ* **112**, 839 (1996)
3. Lintott, C. J., et al., *MNRAS* **389**, 1179 (2008)
4. Cardamone, C., et al., *MNRAS* **339**, 1191 (2009)
5. Amorín, R. O., Pérez-Montero, E., Vílchez, J. M., *ApJ* **715**, L128 (2010)
6. Izotov, Y. I., Guseva, N. G., & Thuan, T. X., *ApJ* **728**, 161 (2011)
7. Pérez-Montero, E., & Contini, T., *MNRAS* **398**, 949 (2009)
8. Overzier, R. A., et al., *ApJ*, **706**, 203 (2009)
9. Erb, D. K., Shapley, A. E., Pettini, M., Steidel, C. C., Reddy, N. A., & Adelberger, K. L., *ApJ*, **644**, 813 (2006)
10. Kakazu, Y., Cowie, L. L., & Hu, E. M., *ApJ*, **668**, 853 (2007)
11. Salzer, J. J., Williams, A. L., & Gronwall, C., *ApJ*, **695**, L67 (2009)
12. Lee, J. C., Salzer, J. J., & Melbourne, J., *ApJ*, **616**, 752 (2004)
13. López-Sánchez, Á. R., *A&A*, **521**, A63 (2010)
14. Kennicutt, R. C., Jr., *ApJ*, **498**, 541 (1998)
15. Meynet, G., & Maeder, A., *A&A*, **390**, 561 (2002)
16. Finlator, K., & Davé, R., *MNRAS*, **385**, 2181 (2008)
17. Dalcanton, J. J., *ApJ*, 658, 941 (2007)
18. Tenorio-Tagle, G., Wünsch, R., Silich, S., & Palouš, J., *ApJ*, **658**, 1196 (2007)
19. Silich, S., Tenorio-Tagle, G., Muñoz-Tuñón, C., Hueyotl-Zahuantitla, F., Wünsch, R., & Palouš, J., *ApJ*, **711**, 25 (2010)
20. Henry, R. B. C., Edmunds, M. G., Köppen, J., *ApJ*, **541**, 660 (2000)
21. Daddi, E., et al., *ApJ*, **670**, 156 (2007)
22. Bournaud, F., & Elmegreen, B. G., *ApJ*, **694**, L158 (2009)
23. Cresci, G., Mannucci, F., Maiolino, R., Marconi, A., Gnerucci, A., & Magrini, L., *Natur*, **467**, 811 (2010)
24. Köppen, J., & Hensler, G., *A&A* **434**, 531 (2005)
25. Papaderos, P., Loose, H.-H., Thuan, T. X., & Fricke, K. J., *A&AS*, **120**, 207 (1996)
26. Cairós, L. M., Vílchez, J. M., González Pérez, J. N., Iglesias-Páramo, J., & Caon, N., *ApJS*, **133**, 321 (2001)
27. Amorín, R., Aguerri, J. A. L., Muñoz-Tuñón, C., & Cairós, L. M., *A&A*, **501**, 75 (2009)